








Article

The Influence of Active Phase Content on Properties and Activity of Nd₂O₃-Supported Cobalt Catalysts for Ammonia Synthesis

Wojciech Patkowski ¹, Magdalena Zybert ^{1,*}, Hubert Ronduda ¹, Gabriela Gawrońska ¹,
Aleksander Albrecht ², Dariusz Moszyński ², Aleksandra Fidler ³, Piotr Dłużewski ³
and Wioletta Raróg-Pilecka ^{1,*}

¹ Faculty of Chemistry, Warsaw University of Technology, Noakowskiego 3, 00-664 Warsaw, Poland

² Faculty of Chemical Technology and Engineering, West Pomeranian University of Technology in Szczecin, Pułaskiego 10, 70-322 Szczecin, Poland

³ Institute of Physics, Polish Academy of Sciences, Al. Lotników 32/46, 02-668 Warsaw, Poland

* Correspondence: magdalena.zybert@pw.edu.pl (M.Z.); wioletta.pilecka@pw.edu.pl (W.R.-P.)

Abstract: A series of neodymium oxide-supported cobalt catalysts with cobalt content ranging from 10 to 50 wt.% was obtained through the recurrent deposition-precipitation method. The effect of active phase, i.e., metallic cobalt, content on structural parameters, morphology, crystal structure, surface state, composition and activity of the catalysts was determined after detailed physicochemical measurements were performed using ICP-AES, N₂ physisorption, XRPD, TEM, HRTEM, STEM-EDX, H₂-TPD and XPS methods. The results indicate that the catalyst activity strongly depends on the active phase content due to the changes in average cobalt particle size. With the increase of the cobalt content, the productivity per catalyst mass increases, while TOF maintains a constant value. The TOF is below average only for the catalyst with the lowest cobalt content, i.e., when the average Co particle size is below 20 nm. This is due to the predominance of strong hydrogen binding sites on the surface, leading to hydrogen poisoning which prevents nitrogen adsorption, thus inhibiting the rate-determining step of the process.

Keywords: cobalt catalyst; ammonia synthesis; neodymium oxide; support; hydrogen poisoning



Citation: Patkowski, W.; Zybert, M.; Ronduda, H.; Gawrońska, G.; Albrecht, A.; Moszyński, D.; Fidler, A.; Dłużewski, P.; Raróg-Pilecka, W. The Influence of Active Phase Content on Properties and Activity of Nd₂O₃-Supported Cobalt Catalysts for Ammonia Synthesis. *Catalysts* **2023**, *13*, 405. <https://doi.org/10.3390/catal13020405>

Academic Editors: Jin-Hyo Boo and Fan Yang

Received: 21 December 2022

Revised: 7 February 2023

Accepted: 11 February 2023

Published: 14 February 2023



Copyright: © 2023 by the authors. Licensee MDPI, Basel, Switzerland. This article is an open access article distributed under the terms and conditions of the Creative Commons Attribution (CC BY) license (<https://creativecommons.org/licenses/by/4.0/>).

1. Introduction

The world's growing population requires more and more food to survive. Increased consumption forces the need to intensify agricultural production based on mineral fertilisers. The primary raw material used to produce mineral fertilisers is ammonia, a nitrogen source. The latest estimates indicate that global ammonia production is increasing by more than 2% annually. In 2020 it reached 150 million tonnes, contributing to the consumption of nearly 2% of the world's energy generated from fossil fuels [1]. Ammonia production is a large-scale catalytic industrial process with significant energy consumption. The compound is obtained directly from gaseous hydrogen and nitrogen [2]. The equilibrium of the reaction requires the use of high temperature and high pressure to obtain economically viable amounts of the product. Due to the high activation energy of the nitrogen molecule, it is necessary to use a catalyst to obtain a sufficiently high reaction rate. Currently, the most used reaction catalyst is a system based on metallic iron, working effectively at a temperature of 400 °C–500 °C and under high pressure, reaching up to 30 MPa in older installations [3]. One of the critical areas of process optimisation is the alleviation of reaction conditions. For this purpose, new catalysts capable of operating effectively under lower pressure and at lower temperatures are designed [4]. Research is focused on developing active catalytic systems based on metals other than iron.

Cobalt, a metal indicated by the volcanic curve, has a high potential for catalysing ammonia synthesis reactions [5]. Starting from the studies of Hagen et al. in 2002 [6,7], a continuously increasing interest in cobalt as the active phase of ammonia synthesis catalysts has been observed. However, obtaining a technologically interesting cobalt catalyst, i.e., one with a satisfactory activity, proper mechanical strength, adequate stability and favourable price, requires optimisation of the catalyst composition in terms of (i) type and properties of the support, (ii) type and content of promoters and (iii) active phase content. Support allows for better use of the catalyst's potential by improving the dispersion of the active phase, stabilising the metal particles on the catalyst surface, influencing the morphology and size of the metal particles and reducing the cost of catalyst production by lowering the amount of the active phase used. This is crucial due to the high and fluctuating price of cobalt as a strategic metal with limited deposits located mainly in politically unstable regions. So far, literature has reported the use of activated carbons [8,9], cerium oxide [10–12] and recently also magnesium oxide [13] or mixed MgO-Ln₂O₃ oxides (Ln = La, Nd, Eu) [14–18] as support for cobalt catalyst. Recent reports also point to such materials as electrides (e.g., C12A7:e[−]) [19] or hydride support materials (e.g., BaH₂) [20] as very effective support promoting ammonia synthesis over a Co-based catalyst. Because cobalt itself is not highly active in the synthesis of ammonia, the addition of selected promoters is also required to increase the catalytic activity of this metal. Barium [21–24] and rare earth metals (especially cerium [25] and lanthanum [26]) must be mentioned among the most effective promoters of cobalt.

The amount of the active phase deposited on the support is also essential. In the case of ammonia synthesis reactions carried out on metals such as cobalt, the reaction's structural sensitivity should be considered. Our previous studies revealed the correlation between the reactivity of the cobalt surface (expressed as TOF) in ammonia synthesis and the particle size of the active phase supported on activated carbon [27]. This, in turn, strongly depends on the amount of active phase. There is an optimal size of cobalt particles (20–30 nm), which ensures the highest activity of the cobalt catalyst in the ammonia synthesis reaction. Increasing or decreasing the particle size caused a decrease in activity, even to the total loss of catalyst activity for fine Co particles (smaller than 0.5 nm). The observed size effect was most likely attributed to changes in Co crystalline structure [27]. However, metal-support interactions and the effect of the amount of active phase loaded on the support on its particle size as well as exposed surface area, and catalytic activity, are usually specific to each catalytic system. In the case of the carbon support, increasing the amount of cobalt introduced to the range of 4.9–67.7 wt.% resulted in a significant increase in the size of cobalt particles in the range of 3–45 nm [27]. However, when cobalt was deposited on the mixed MgO-La₂O₃ support in the amount of 10–50 wt.%, the size and structure of Co nanoparticles in the catalysts remained nearly unchanged despite the fivefold increase in the Co loading amount [28].

The study presented in this paper aimed to investigate the influence of active phase, i.e. metallic cobalt content on the properties and activity of Nd₂O₃-supported cobalt catalysts for ammonia synthesis. As reported in the previous studies [29–32], rare earth metal oxides were effective supports of the ruthenium catalyst for ammonia synthesis. Niwa et al. [29] showed that the use of rare-earth metal oxides as supports is more effective than using their cations in the role of promoters. Ruthenium catalysts deposited on rare-earth metal oxides were almost twice as active as the reference systems (Ru/MgO) promoted with the rare-earth metal cations. The increased activity was attributed to Strong Metal-Support Interactions (SMSI). Miyahara et al. [30] revealed different activities of ruthenium catalysts depending on the support used, with higher activity characterising catalysts deposited on lighter oxides according to the following trend: Pr₂O₃ > CeO₂ > La₂O₃ > Nd₂O₃ > Sm₂O₃ > Gd₂O₃. The high activity of the Ru/Pr₂O₃ system was explained by Sato et al. [31] due to the favourable morphology of the catalyst surface in the form of a ruthenium nanolayer rich in defects and terraces, structurally similar to the active B5 sites. Additionally, the high alkalinity of the support was conducive to

effective charge transfer to the metal surface and facilitated the dissociation of the adsorbed N_2 molecule (a rate-determining step of the NH_3 synthesis reaction). During kinetic studies of the Ru/ Pr_2O_3 catalyst, Imamura et al. [32] also indicated high resistance to hydrogen and product poisoning, unlike Ru systems based on carbon or oxide supports. These studies were an inspiration to use rare-earth metal oxides as supports for cobalt catalysts for ammonia synthesis. Neodymium oxide was also selected based on our previous studies [18], where Nd_2O_3 had the most favourable effect on the catalytic properties of cobalt systems supported on mixed $MgO-Ln_2O_3$ oxides (where $Ln = La, Nd, Eu$).

In the present work, a series of cobalt catalysts containing 10–50 wt.% of cobalt supported on neodymium oxide was prepared. The activity of the catalysts with different Co loading was tested in ammonia synthesis at 470 °C under the pressure of 6.3 MPa. The detailed characterisation studies using N_2 physisorption, X-ray powder diffraction (XRPD), microscopic methods (TEM, HRTEM, STEM-EDX), X-ray photoelectron spectroscopy (XPS) and temperature-programmed desorption (H_2 -TPD) were conducted to understand the effect of active phase content on catalyst structural parameters, morphology, crystal structure and surface state, as well as composition and activity of the catalysts.

2. Results and Discussion

Table 1 lists the textural parameters (specific surface area, S_{BET} , and the total volume of pores, V_{por}) of catalyst precursors determined using N_2 physisorption. All systems display a relatively developed specific surface area. Increasing the cobalt loading causes an expansion of the S_{BET} area of the catalyst precursor. In the case of subsequent systems, the specific surface area increase is logarithmical, yielding diminishing growth for every additional wt.% increase in the Co content of the precursor. The porosity of the precursors follows the growth trend of the surface area.

Table 1. Textural parameters of cobalt catalyst precursors.

| Parameter | Co(10)/ Nd_2O_3 | Co(19)/ Nd_2O_3 | Co(31)/ Nd_2O_3 | Co(39)/ Nd_2O_3 | Co(50)/ Nd_2O_3 |
|---|-------------------|-------------------|-------------------|-------------------|-------------------|
| Specific surface area S_{BET} ¹ [$m^2 g^{-1}$] | 27.3 | 32.0 | 36.5 | 39.6 | 41.8 |
| Total pore volume V_{por} ² [$cm^3 g^{-1}$] | 0.104 | 0.125 | 0.132 | 0.139 | 0.142 |

¹—estimated based on the BET isotherm. ²—estimated based on the BJH isotherm.

Figure 1a depicts the N_2 physisorption isotherms registered for catalyst precursors. All registered curves are of type II shape, indicating that precursors are predominantly macroporous materials. Increasing cobalt content does not change the isotherm shape. However, they shift upward to higher total adsorbate volumes. This observation, combined with the fact that the Nd_2O_3 , used as support is non-porous and of low surface area (ca. $2 m^2 g^{-1}$), indicates that the porosity may be attributed to the structures formed by cobalt oxide. Therefore, depositing subsequent layers of cobalt compounds on the surface of the output catalyst precursor leads to the expansion of the existing porous structure without changing its nature. Also, all curves contain a hysteresis loop of H3 type caused by capillary condensation in mesopores. Its presence suggests that cobalt oxide forms the aggregates of plate-like particles giving rise to wedge- or slit-shaped pores. With increasing cobalt content in the precursor, the area of the loop increases, indicating an intensification of the capillary condensation phenomenon, thus increasing mesopore total volume. Figure 1b depicts the pore volume distribution of the precursors. The curves indicate that these are porous materials with bimodal pore volume distribution. The porous structure is formed by numerous pores in the 20–80 nm diameter range and macropores with sizes above 80 nm. The materials contain a very small number of micropores.

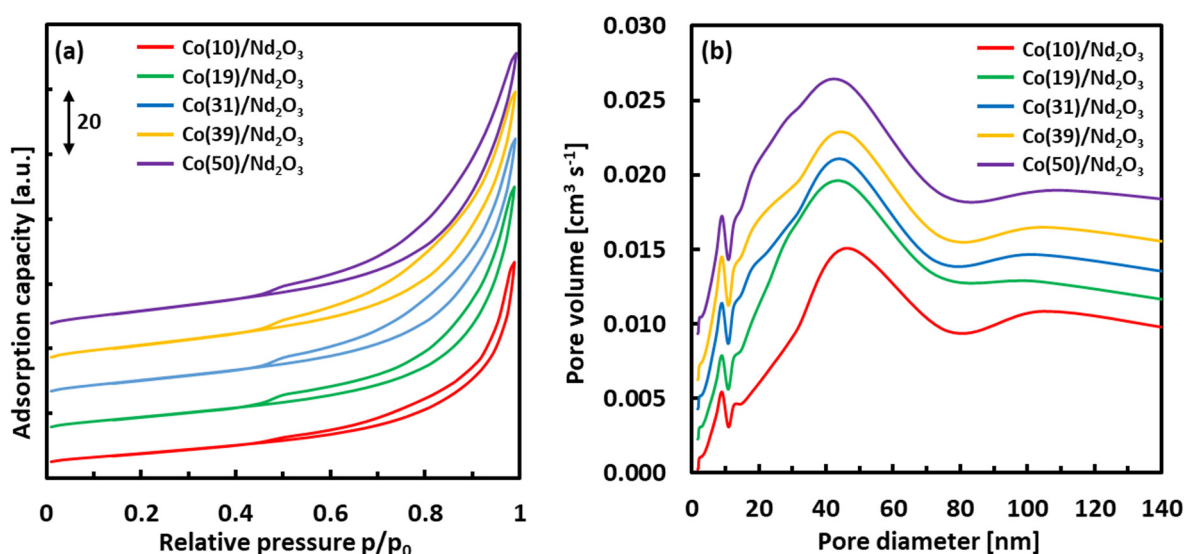


Figure 1. N_2 physisorption isotherms (a) and pore volume distribution (b) of cobalt catalyst precursors.

X-ray powder diffraction studies (XRPD) were carried out to determine the phase composition of catalysts. Figure 2 depicts patterns of cobalt catalyst in the form of a precursor and in-situ reduced form.

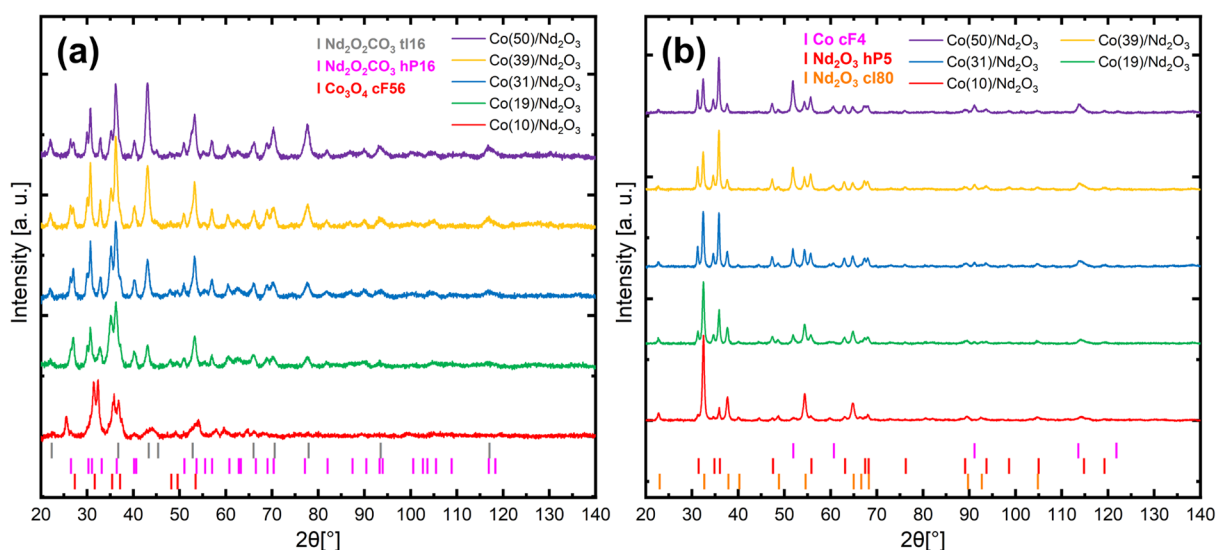


Figure 2. XRPD patterns of the cobalt catalysts supported on neodymium oxide (Co/Nd_2O_3) in the form of a precursor (a) and the in-situ reduced form (b).

The phase composition of all catalyst precursors (Figure 2a) is very similar. On most patterns, one can observe distinct Bragg's reflections indicating the presence of Co_3O_4 spinel with a cubic structure (PDF-4+ 2021 04-003-0984). The presence of this phase cannot be unambiguously demonstrated for the $Co(10)/Nd_2O_3$ system due to the overlapping of reflection profiles. The intensity of reflections from the Co_3O_4 phase for systems with increasing cobalt content increases. The calculated mean crystallite size of the Co_3O_4 phase is generally independent of the cobalt content and is in the range of 11–12 nm. No signals from Nd_2O_3 (the support) are observed on the precursor patterns. Instead, reflections attributed to neodymium dioxycarbonates $Nd_2O_2CO_3$ with tetragonal (PDF-4+ 2021 00-025-0567) and hexagonal structure (PDF-4+ 2021 04-009-3412) are visible. This is due to the conditions under which the catalyst precursors were synthesised. The high-temperature water environment rich in CO_3^{2-} ions enabled the formation of dioxycarbonates [33,34].

Figure 2b depicts the diffraction profiles of in-situ reduced Co/Nd₂O₃ catalysts at ambient temperature. As a result of the reduction process, a disappearance of reflections attributed to the Co₃O₄ spinel occurs. This results in reflections from the cobalt metallic phase of the cubic face-centred structure (PDF-4+ 2021 01-077-7452) present in the patterns. A detailed description of these reflections is difficult because their location coincides with numerous reflections generated by the support phases. Increasing the cobalt loading in the catalyst leads to an increase in the metallic Co phase concentration and thus intensities of Co reflections. All measurements showed similar cobalt mean crystallite size resulting from analysis based on the Rietveld method. As a result of catalyst reduction, the complete disappearance of reflections attributed to polymorphic Nd₂O₂CO₃ is also observed. The decomposition of dioxycarbonates leads to the exposure of support structures, in this case Nd₂O₃ [35]. In Figure 2b, sets of reflections are observed, indicating the presence of two phases of neodymium oxide with different crystal structures in the material: regular (PDF-4+ 2021 03-065-3184) and hexagonal (PDF-4+ 2021 01-072-8425).

The phase analysis presented above indicates that cobalt is present as cobalt oxide Co₃O₄ in the precursors, which is then completely reduced to metallic cobalt during the precursor activation. In the case of other similar catalytic systems in which cobalt was deposited on the surface of oxide support, such as the Co/Mg-La system [14,28], incomplete reduction of cobalt compounds contained in the catalyst were observed. For this reason, the surface composition of the catalysts in both precursor and active forms was investigated by X-ray photoelectron spectroscopy (XPS).

The presence of cobalt, neodymium, oxygen and slight adventitious carbon contamination was indicated on the surface of the precursors. After the reduction process, cobalt, neodymium and oxygen remained on the surface. Figure 3 shows the XPS spectrum of the Co 2p detailed region for the precursor and active form of the Co(10)/Nd₂O₃ catalyst. The figure also shows the result of the deconvolution of the XPS spectra for both samples, based on the method presented in the work of Biesinger et al. [36]. The components of the XPS Co 2p lines originating from the precursor are marked with thin lines. The components coming from the catalyst after the precursor reduction process are highlighted as grey areas. The location of the maximum of the Co 2p_{3/2} peak at a binding energy of 780 eV indicates the presence of cobalt oxides on the surface of the precursor. In the binding energy region from 784 eV to 793 eV, characteristic satellites appear in the spectrum of the Co 2p detailed region. Based on the envelope shape of the Co 2p peaks, the presence of Co₃O₄ oxide can be ascertained [36], previously confirmed by analysis based on X-ray diffraction studies.

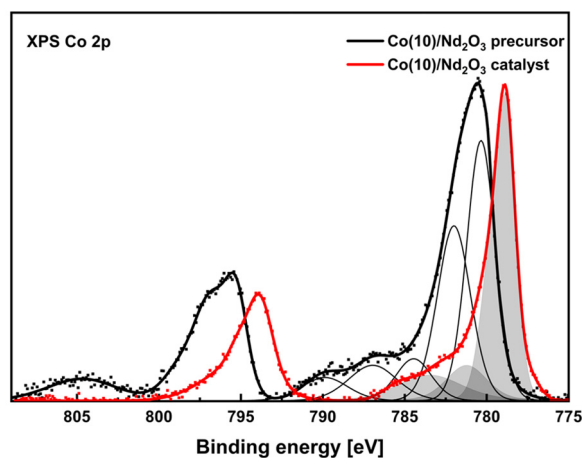


Figure 3. XPS Co 2p spectra of Co(10)/Nd₂O₃ precursor and catalyst after reduction. The components of the Co 2p lines are marked with thin solid lines for the precursor and grey areas for the reduced catalyst.

The exposure of precursors to hydrogen at elevated temperatures results in the process of reduction of cobalt oxides [37]. In Figure 3, a shift in the maximum of the Co 2p line from the 780 eV position to 778 eV, corresponding to the reduction of cobalt oxides to metallic cobalt, is observed. No surface cobalt oxides are observed in any samples analysed after their reduction process in hydrogen. Therefore, it should be concluded that cobalt exists exclusively in metallic form in the tested catalysts, which was confirmed by X-ray studies.

The selected catalysts of the lowest (Co(10)/Nd₂O₃), medium (Co(31)/Nd₂O₃) and highest (Co(50)/Nd₂O₃) cobalt content were examined using transmission electron microscopy (TEM), high-resolution transmission electron microscopy (HRTEM), scanning transmission electron microscopy (STEM) and energy dispersive X-rays (EDX) analysis. These examinations were used to obtain information about the morphology of the systems, the size distribution of the cobalt particles and their crystal structure.

TEM images registered for the cobalt catalysts (Figure 4) indicate that all systems display similar structures and morphology. Most materials are homogenous and form agglomerates of particles of size ranging from 20 to 100 nm. These agglomerates consist of particles that are not tightly packed together, and distances among them do not exceed 100 nm. These results agree with the pore size distribution obtained through the N₂ physisorption measurements, assuming the morphology of the samples does not change significantly due to the reduction process.

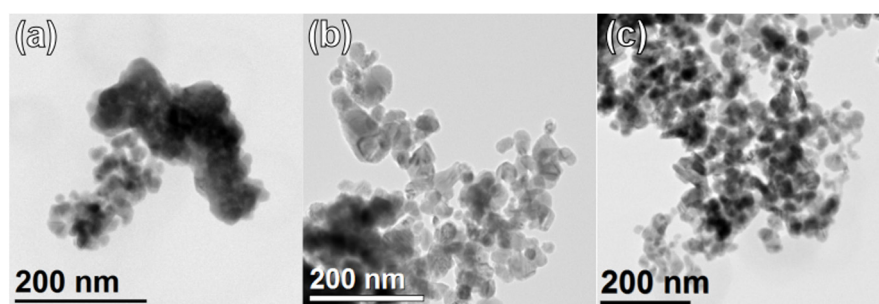


Figure 4. TEM images of regions of the Co(10)/Nd₂O₃ (a), Co(31)/Nd₂O₃ (b), Co(50)/Nd₂O₃ (c) catalysts.

Figure 5 depicts the HRTEM images of Co crystallites in the selected cobalt catalysts. The structure of cobalt crystallites was identified based on the analysis of the 2D-FT images from the selected areas. It was determined that for all cobalt crystals observed, the interplanar distances and the angle between them correspond to 0.207 nm and 70.5°, respectively, describing the (-111) and (-11-1) planes of the cobalt face-centred cubic structure (*Fm-3m* space group). The structure in question (ICSD 760020) is characterised by the unit cell parameter $a = 0.3578$ nm. Figure 5a also depicts that the observed Co crystallite in the Co(10)/Nd₂O₃ system is covered with a thin (ca. 2 nm) layer of CoO. The presence of the layer results from the partial oxidation of the Co crystallite caused by the nature of the ex-situ measurements. Based on the HRTEM and FT images from area no. 2, it was found that the interplanar distances and the angle between them are equal to 0.246 nm, 0.213 nm and 54.7°, respectively, corresponding to the (1-11) and (002) planes of the face-centred cubic CoO structure (space group *Fm-3m*). The unit cell parameter for the CoO structure (ICSD 245324) $a = 0.4264$ nm. The phenomenon of partial surface oxidation was also observed in the case of several Co crystallites in the other systems that underwent HRTEM investigation. It is worth noting that the face-centred cubic structure is the only type of cobalt structure observed in high-resolution images of all Co/Nd₂O₃ systems, which is consistent with the XRPD analysis results.

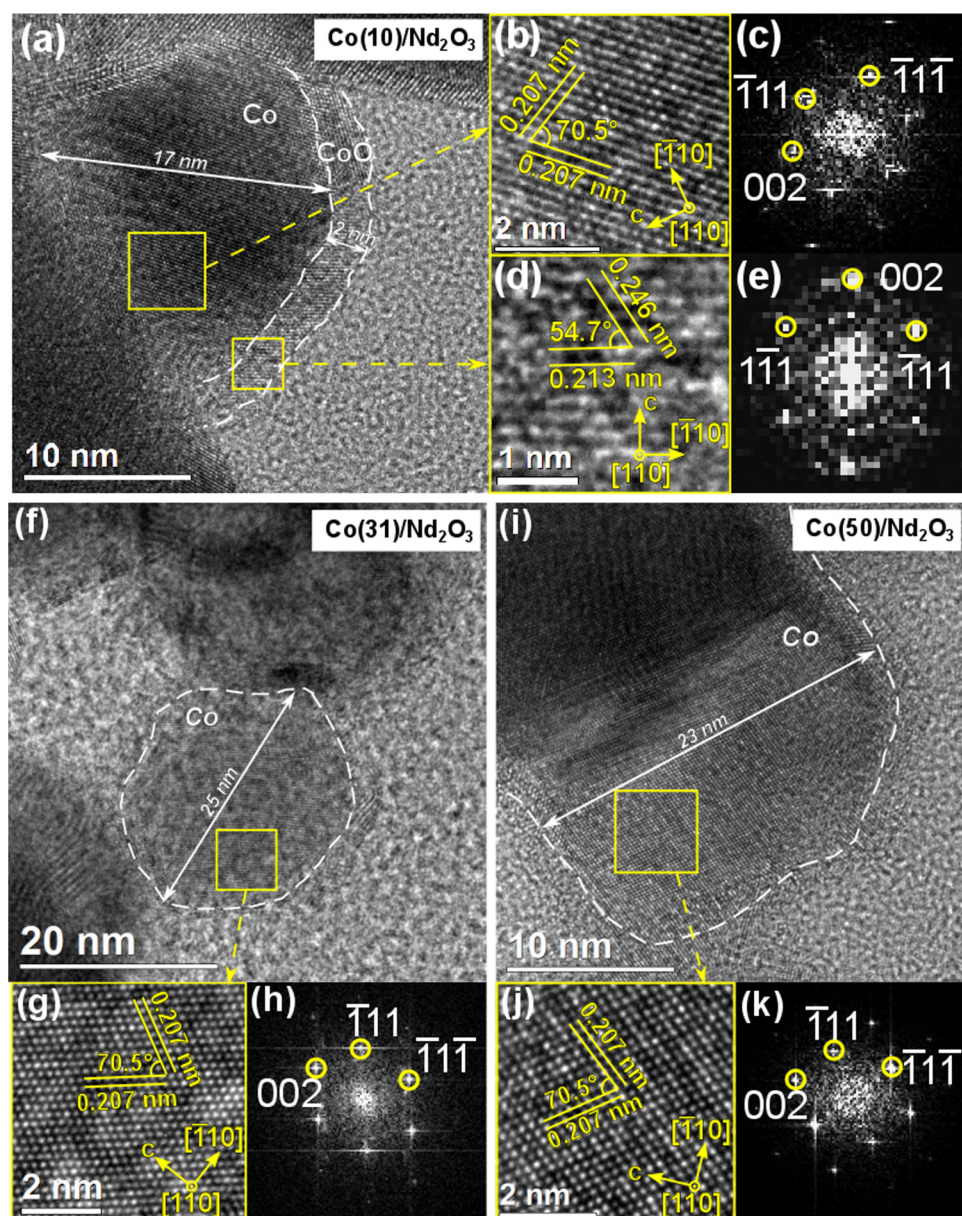


Figure 5. HRTEM images of exemplary Co crystallites (a,f,i) and magnified images of highlighted regions of the Co crystallites (b,g,j) and CoO layer (c) with corresponding Fourier transform (FT) (d,e,h,k). Yellow circles mark the reflections on the FT generated by the indicated crystal planes.

The composition and distribution of elements in the Co/Nd₂O₃ systems were obtained by STEM imaging coupled with EDX analysis. Mapping results are presented in Figure 6. The images show that for the Co(10)/Nd₂O₃ system, single Co particles are uniformly distributed over the Nd₂O₃ support, but their random agglomeration can be observed. With the increase of the Co loading in the catalyst, the particle distribution becomes less uniform. For the Co(31)/Nd₂O₃ system, Co particles are very densely distributed in some areas of the support surface, forming clusters exceeding 100 nm in size. In other regions, however, single particles of the active phase can be distinguished. For the Co(50)/Nd₂O₃ system, the cobalt particle compaction with the increasing cobalt loading continues and they are very densely distributed on the Nd₂O₃ support. Their distribution, however, is quite uniform; most of the particles form tightly packed agglomerates with only a few individual Co particles visible. With the increase in the cobalt content, the average size of metal particles increases. This observation, combined with the visible agglomeration, may

indicate that Nd_2O_3 does not exert a structural influence on the cobalt phase. In contrast, the effect of prevention of particles from agglomeration and sintering was observed for the other rare-earth oxides used as supports or promoters of cobalt catalysts, namely La_2O_3 [26,38] and CeO_2 [21,25,39].

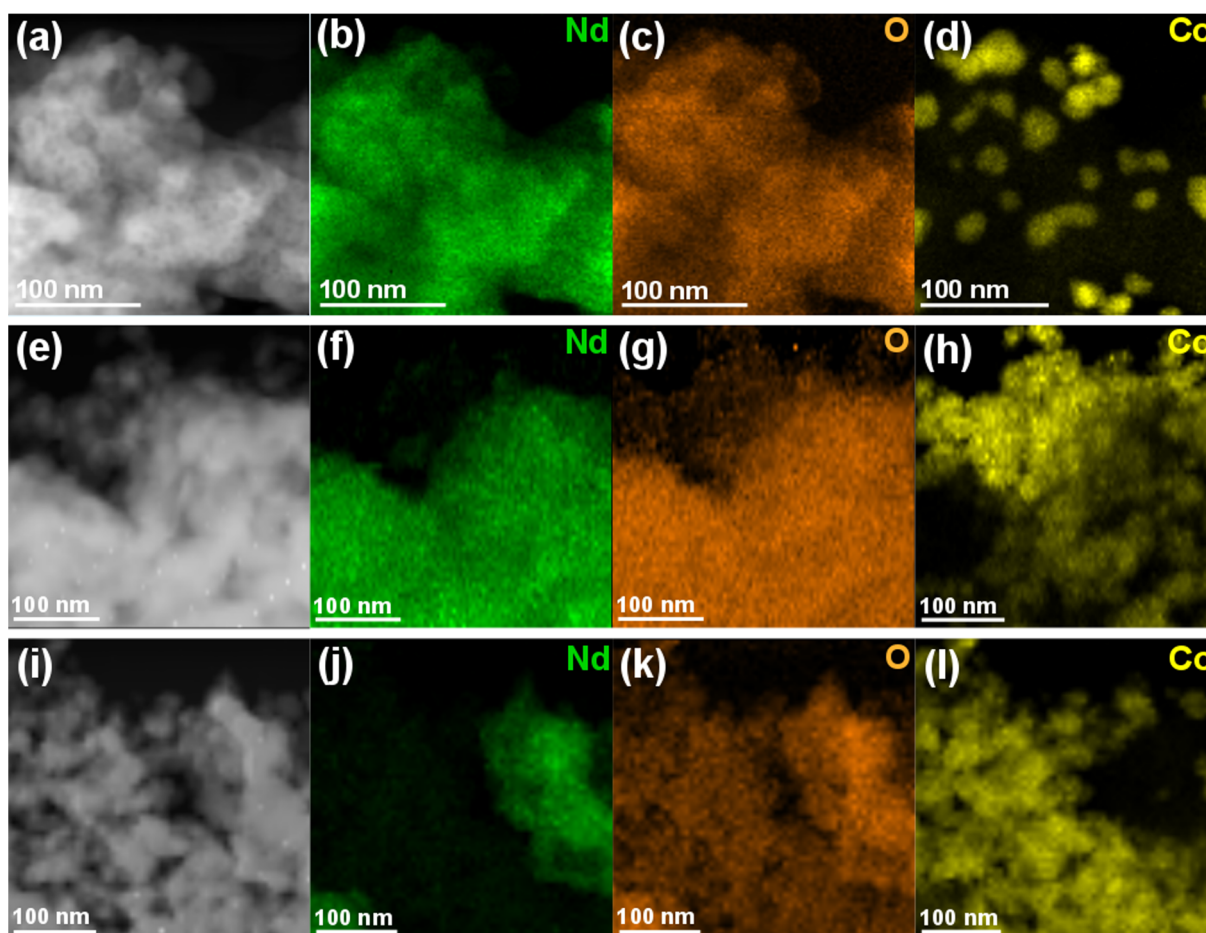


Figure 6. STEM images (first column) and corresponding elemental EDX mappings of the $\text{Co}(10)/\text{Nd}_2\text{O}_3$ (a–d), $\text{Co}(31)/\text{Nd}_2\text{O}_3$ (e–h), $\text{Co}(50)/\text{Nd}_2\text{O}_3$ (i–l) catalysts, showing Nd (green), O (orange) and Co (yellow) concentrations.

Figure 7 depicts hydrogen desorption profiles recorded for reduced $\text{Co}/\text{Nd}_2\text{O}_3$ catalysts. A very similar bimodal character describes all registered desorption profiles. Both low- (LT) and high-temperature (HT) peaks can be distinguished in each profile, the area of which gradually changes between systems with increasing active phase content. The first observed signal contributing to the formation of an atypical low-temperature peak is a small local signal occurring at 50°C , corresponding to the desorption of hydrogen weakly bound to the catalyst surface. The main low-temperature peak, corresponding to the presence of adsorption centres with low hydrogen binding energy, consists of overlapping peaks with maxima located at 150°C for the $\text{Co}(10)/\text{Nd}_2\text{O}_3$ system and at 100°C for the others. The intensity of these signals increases significantly for subsequent systems in the series, along with the increasing content of the active phase. The irregular shape of the low-temperature peak indicates some variation in the hydrogen binding centres, all with relatively low binding energy [39,40]. The low-temperature signal disappears and systematically shifts into a high-temperature signal at 400°C – 500°C . The signal above this temperature consists of a single wide peak indicating the presence of high-energy binding sites on the catalyst surface. Its area and maximum temperature differ between the systems. In the case of the $\text{Co}(10)/\text{Nd}_2\text{O}_3$ profile, its maximum is located at 715°C . The

peak has the largest area and a symmetrical shape. The high-temperature signal of other systems is weaker, which, when combined with the lack of such a clear maximum, may suggest fewer centres strongly binding hydrogen. A temperature shift of the maximum of the high-energy peak is also observed from 765 °C for Co(19)/Nd₂O₃ to approximately 700 °C for the Co(50)/Nd₂O₃ system, indicating the weakening of their average strength.

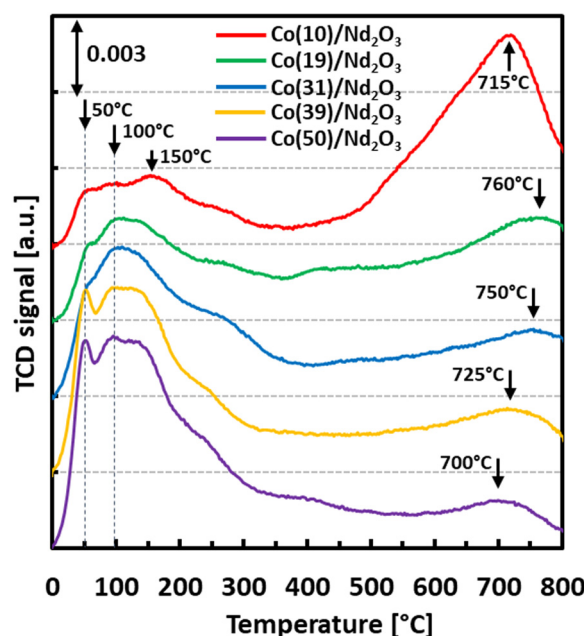


Figure 7. H₂-TPD profiles for Co/Nd₂O₃ catalysts.

Table 2 presents the measured volume of hydrogen desorbed from the catalyst surface and the share of low and high-temperature signals in the total volume. While the total volume of desorbed H₂ does not vary significantly between the samples and oscillates in the range of 1.7–2 cm³ g^{−1}, the share of the particular signals changes notably. With the increase of Co loading, the high-temperature peak share decreases and that of the low-temperature peak increases. Consequently, for the Co(10)/Nd₂O₃, the majority of the hydrogen desorbed is generated by the strong binding sites, while for the Co(50)/Nd₂O₃, the hydrogen comes mostly from weakly binding sites. Table 3 presents the average cobalt (i.e., the active phase) particle size determined through H₂-TPD and a comparison of these values to TEM and XRPD-derived data.

Table 2. The total volume of hydrogen desorbing from the catalyst surface and the proportion of low- and high-temperature peak contribution.

| Parameter | Co(10)/Nd ₂ O ₃ | Co(19)/Nd ₂ O ₃ | Co(31)/Nd ₂ O ₃ | Co(39)/Nd ₂ O ₃ | Co(50)/Nd ₂ O ₃ |
|--|---------------------------------------|---------------------------------------|---------------------------------------|---------------------------------------|---------------------------------------|
| Total hydrogen volume [cm ³ g ^{−1}] | 1.99 | 1.82 | 1.68 | 1.82 | 2.02 |
| Low-temperature peak (LT) share [%] | 26 | 43 | 68 | 75 | 86 |
| High-temperature peak (HT) share [%] | 74 | 57 | 32 | 25 | 14 |

Table 3. Comparison of average Co particle and Co crystallite size in the Co/Nd₂O₃ catalysts, determined through H₂-TPD, XRPD and TEM.

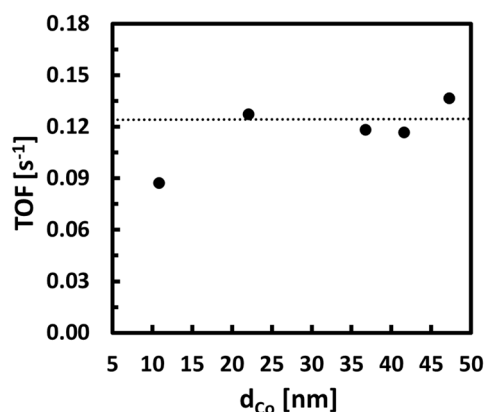
| Parameter | Co(10)/Nd ₂ O ₃ | Co(19)/Nd ₂ O ₃ | Co(31)/Nd ₂ O ₃ | Co(39)/Nd ₂ O ₃ | Co(50)/Nd ₂ O ₃ |
|--------------------------|---------------------------------------|---------------------------------------|---------------------------------------|---------------------------------------|---------------------------------------|
| d _{H2-TPD} [nm] | 11 | 22 | 37 | 42 | 47 |
| d _{STEM} [nm] | 27 | - | 36 | - | 51 |
| d _{XRPD} [nm] | 17 | 21 | 21 | 20 | 19 |

The data indicates that the average size of Co particles increases with cobalt loading in Co/Nd₂O₃ catalysts. The size growth is nonlinear, but the deviation from a direct proportionality is marginal. The average particle sizes calculated based on chemisorption data are in good accordance with the sizes measured during STEM-EDX observations. However, they are different from the uniform sizes calculated based on diffraction data, which may be caused by the cobalt particles being polycrystalline. The sole existence of the face-centred cubic phase supports the polycrystallinity of cobalt particles. It is in good agreement with the fact that ca. 20 nm and smaller cobalt crystallites tend to occur predominantly in the cubic phase [41]. Without additional structural stabilisation, little to no hexagonal phase is present. It is because in temperatures above 427 °C (i.e., in temperatures lower than the temperature of the activation or the NH₃ synthesis reaction), cobalt, which naturally tends to prevail in the hexagonal close-packed phase [42], undergoes an allotropic transition into the face-centred cubic structure [43].

Activities of Co/Nd₂O₃ catalysts are presented in Table 4. With the increase of cobalt loading, the average reaction rate per catalyst unit mass increases. However, it is worth noting that the observed increase is not directly proportional. The active phase mass increases 5 times, resulting in a less than 2 times increase in average reaction rate. It means that despite the incremental increase of the catalyst surface area and an increase in the number of active sites, the overall efficiency of their utilisation gradually decreases. It is supported by the activity data indicating that for most of the systems, the surface activity is roughly similar, and TOF averages ca. 0.125 s^{−1} (see Figure 8); thus, the influence of the support on the active phase is relatively constant in the studied Co loading range.

Table 4. The activity of Co/Nd₂O₃ catalysts in ammonia synthesis reaction expressed as the average reaction rate (*r*_{avg}) and TOF.

| Parameter | Co(10)/Nd ₂ O ₃ | Co(19)/Nd ₂ O ₃ | Co(31)/Nd ₂ O ₃ | Co(39)/Nd ₂ O ₃ | Co(50)/Nd ₂ O ₃ |
|--|---------------------------------------|---------------------------------------|---------------------------------------|---------------------------------------|---------------------------------------|
| <i>r</i> _{avg} [g _{NH3} g _{cat} ^{−1} h ^{−1}] | 1.01 | 1.39 | 1.27 | 1.42 | 1.82 |

**Figure 8.** Surface activity (TOF) of Co/Nd₂O₃ catalysts vs Co particle average size. The dotted line represents the average activity level of catalysts. Large dots represent particle sizes calculated on the basis of H₂-TPD results (d_{H2-TPD}, vide Table 3).

However, one may observe that the surface activity of the Co(10)/Nd₂O₃ catalyst is lower than the average TOF displayed by the others. This state is depicted in Figure 8. It may be related to the smaller size of cobalt particles in this system. Recent studies of cobalt systems deposited on active carbon indicated the optimal cobalt particle size range (20–30 nm) provided the highest activity in ammonia synthesis [27]. Studies of cobalt systems deposited on mixed MgO–La₂O₃ oxides also showed that cobalt particles of 20 nm of average size yield the highest reaction rate [28].

Our results indicate that when the size of the active phase (metallic cobalt) particles decreases in a Co/Nd₂O₃ system, the strength of hydrogen binding by the surface increases (Figure 9) as the high-energy to low-energy binding sites ratio grows exponentially. It may seem that when the size of cobalt particles decreases below a certain critical value, i.e., of 20 nm, the above ratio exceeds 1.5 due to the predominance of sites binding hydrogen strongly on the catalyst surface. With the decrease in cobalt particle sizes, more undercoordinated structures, such as close-packed terraces, steps, kinks etc., occur at the cost of open surfaces [41]. These structures bind hydrogen more strongly than flat surfaces [44,45]. Under these circumstances, hydrogen poisoning of the active phase may occur, limiting the activity of the catalyst. Strongly-bound hydrogen blocks the active sites, preventing nitrogen adsorption [14,46–49] and thus inhibiting the rate-determining step of the process [50–53].

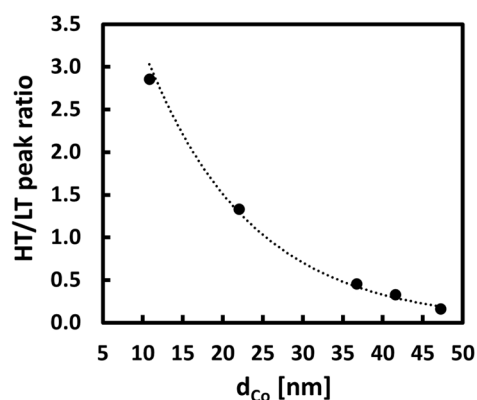


Figure 9. Correlation between the high- and low-temperature H₂ desorption peak ratio and Co particle average size of the Co/Nd₂O₃ catalysts. Large dots represent particle sizes calculated on the basis of H₂-TPD results (d_{H_2-TPD} , vide Table 3).

3. Materials and Methods

3.1. Catalyst Preparation

The first stage of the catalyst preparation was the calcination of the Nd₂O₃ support (UMSC Lublin, Poland, 99.99% purity) in the air at 800 °C for 16 h to purify the material by decomposing any neodymium hydroxides and carbonates present [54–56]. Cobalt catalyst precursors were synthesised by the recurrent deposition-precipitation method. The target cobalt content in the catalyst was set in the range of 10 to 50 wt.% at 10 wt.% increments. The systems were labelled as Co(X)/Nd₂O₃, where X represents the actual cobalt content in the active form of the catalyst. Cobalt(II) carbonate was precipitated with K₂CO₃ (Avantor Performance Materials Poland S.A., Gliwice, Poland) from an aqueous solution of (Co(NO₃)₂·6H₂O (Acros Organics, Thermo Fischer Scientific, Kandel, Germany) onto the Nd₂O₃ suspension. The synthesis was conducted at a double molar excess of the precipitating reagent relative to the amount of cobalt nitrate salt. The solution temperature was 85 °C and a mixing speed of 500 rpm was used. The precipitation process was continued until pH = 9 was established, and then the mixture was aged for 1 h. After ageing, the solution was cooled to room temperature and filtered at a reduced pressure ($p = 50$ mbar). Then the precipitate was washed with distilled water from the residues of potassium, nitrate and carbonate ions to a pH ≈ 7 of the filtrate. The purified sludge

was dried for 24 h at 120 °C. Obtained materials were calcined in air at 500 °C for 5 h. A neodymium oxide suspension was used as a substrate only for the synthesis of the first Co(10)/Nd₂O₃ precursor system. For the subsequent Co(X)/Nd₂O₃ systems, the precursor form of the Co(X-10)/Nd₂O₃ system was used as the suspension on which another portion of cobalt(II) carbonate was deposited. The cobalt carbonate deposition process was repeated in a precipitation-calcination cycle, increasing the cobalt content by the assumed value of 10 wt.%. The precursors were then tabletted, crushed and sieved to obtain a grain fraction of 0.2–0.63 mm. Fractioned precursors were later subjected to the in-situ activation (reduction) procedure directly before the measurements that required a reduced form of the catalyst. The composition of the obtained catalysts in the reduced (active) form, i.e., metallic cobalt deposited on neodymium oxide, is presented in Table 5.

Table 5. Composition of reduced cobalt catalysts determined with ICP-AES.

| Parameter | Co(10)/Nd ₂ O ₃ | Co(19)/Nd ₂ O ₃ | Co(31)/Nd ₂ O ₃ | Co(39)/Nd ₂ O ₃ | Co(50)/Nd ₂ O ₃ |
|-------------------|---------------------------------------|---------------------------------------|---------------------------------------|---------------------------------------|---------------------------------------|
| Co content [wt.%] | 9.9 | 19.4 | 30.8 | 38.6 | 49.6 |
| Nd content [wt.%] | 77.2 | 65.6 | 59.6 | 46.8 | 39.5 |

3.2. Characterisation Methods

Textural parameters of the catalyst precursors were determined by N₂ physisorption (Micromeritics Instrument Co., Norcross, GA, USA). Before the measurement, each sample of ca. 0.5 g was evacuated under vacuum $p < 100 \mu\text{mHg}$ for 1 h at 90 °C and then for the next 4 h at 300 °C. The specific surface area (S_{BET}) of all the materials was determined based on a five-point measurement in the $p/p_0 = 0.01$ –0.3 relative pressure range approximated with the Brunauer–Emmett–Teller (BET) isotherm. The total pore volumes (V_{por}) were determined based on the multipoint measurement in the $p/p_0 = 0.01$ –1 relative pressure range approximated with the Barrett–Joyner–Halenda (BJH) isotherm and were defined for $p/p_0 = 0.995$.

Temperature-programmed hydrogen desorption (H₂-TPD) was carried out with the AutoChem 2920 (Micromeritics Instrument Co., Norcross, GA, USA) equipped with a TCD detector, using U-shaped quartz reactors and utilising high purity ($\geq 6 \text{ N}$) gases. H₂-TPD profiles were captured for reduced catalyst samples. The reduction was carried out in-situ for 16 h at 550 °C in the H₂ flow ($40 \text{ cm}^3 \text{ min}^{-1}$). After the reduction process, the samples were rinsed with an inert gas at 620 °C for 1 h and then cooled to 0 °C. Hydrogen was adsorbed during cooling from 150 °C to 0 °C and for 15 min at 0 °C. Then the samples were rinsed with Ar for 60 min to eliminate physisorbed H₂. Next, hydrogen desorption was conducted during a temperature increase from 0 °C to 800 °C at a heating rate of 10 °C min^{-1} . The concentration of the desorbed hydrogen was measured with a TCD. The desorption profiles were used to calculate the amount of hydrogen desorbed from the metallic Co surface and to estimate the active phase average particle size (assuming the stoichiometry of H₂ adsorption on cobalt H:Co = 1:1) [57,58].

The X-ray powder diffraction method (XRPD) determined the phase of precursors and catalysts in the reduced form. The diffraction measurements of catalyst precursors and their active forms were performed in-situ on an X'Pert PRO MPD diffractometer (Philips PANalytical, Almelo, The Netherlands) using CoK α radiation, operating in a Bragg–Brentano configuration, coupled to an XRD 900 reaction chamber (Anton Paar, Graz, Austria). The diffraction data were collected in the 2θ scattering range of 20°–90°, with 0.02° step size and 400 s count time per step. Crystalline phase identification was performed using the PANalytical High Score Plus software with the ICDD PDF4+ 2021 database. The weight concentrations of individual crystalline phases were determined based on full-range refinement of the diffraction profile using the Rietveld method. The catalysts were reduced in an H₂ (N5.0, Messer, Warszawa, Poland) stream, with a flow rate of $100 \text{ cm}^3 \cdot \text{min}^{-1}$, at a

temperature of 500 °C for 10 h. Diffraction analyses of both catalyst precursors and their active forms were carried out at an ambient temperature.

The X-ray photoelectron spectroscopy (XPS) analysis was carried out for the oxide precursors and the reduced samples. The measurements were conducted using Al K α ($h\nu = 1486.6$ eV) radiation in a PreVac (Rogów, Poland) system equipped with Scienta SES 2002 electron energy analyser operating at constant transmission energy ($E_p = 50$ eV). The reduction of precursors was conducted in a High-Pressure Cell (HPC) of an ultra-high vacuum (UHV) system. A small tablet of a sample, approximately 10 mm in diameter, was placed on a sample holder and introduced into HPC. Hydrogen (N5.0 Messer, Poland) was passed through the sample at a constant flow of $20\text{ cm}^3\cdot\text{min}^{-1}$. The sample was heated to 500 °C. The reduction was carried out for 5 h. The sample was then transferred under UHV to the analysis chamber of the electron spectrometer.

TEM investigation of specimens of spent catalysts was carried out using an FEI Titan Cubed 80-300 (FEI Technologies Inc., Hillsboro, OR, USA) microscope operating at 300 kV with a point resolution of 70 pm. The overview images were registered in bright-field TEM mode at magnifications ranging from $7100\times$ to $31,000\times$, while the HRTEM images were collected at magnifications from $340,000\times$ to $520,000\times$. The Gatan BM-Ultrascan CCD (Gatan Inc., Pleasanton, CA, USA) camera was used to record both types of images. STEM images were recorded using a HAADF detector and the elemental mapping of the samples was obtained using the in-situ EDX spectrometer. The test material (0.5 mg) was suspended in ethanol (2 mL) and sonicated for 60 s. A drop (20 μL) of the suspension was deposited on a standard TEM copper grid with a diameter of 3 mm, coated with a 30 nm thick amorphous carbon film (EM Resolutions Ltd., Sheffield, UK). After the complete evaporation of the alcohol, the grid was ready for microscopic observations.

Catalytic activity measurements in the ammonia synthesis reaction of Co/Nd₂O₃ catalysts were carried out in a tubular flow reactor supplied with a very pure (99.99995 vol.%) H₂/N₂ = 3 stoichiometric mixture (gas flow rate $70\text{ dm}^3\text{ h}^{-1}$) under semi-industrial conditions: temperature of 470 °C and pressure of 6.3 MPa. A detailed description of the apparatus used can be found elsewhere [15,59]. Before the measurements, the catalyst samples were activated under atmospheric pressure in the reacting gas mixture consecutively at 470 °C for 72 h, then 520 °C for 24 h and 550 °C for 48 h. The outlet concentration of ammonia was measured using an interferometer. The catalytic activity was determined and expressed as an average reaction rate based on the measurement results. Moreover, based on the chemisorption data and activity measurements, an activity of the catalyst's surface (expressed as TOF value) was calculated.

4. Conclusions

In summary, a series of Nd₂O₃-supported Co catalysts of various active phase (metallic cobalt) loading (10–50 wt.%) were synthesised with recurrent deposition precipitation, characterised and tested in NH₃ synthesis. The increase in productivity with the increase in cobalt content was observed in the entire loading range. The increase was linear, however it was disproportionately smaller than the increase in the active phase content. Despite this, catalyst TOF was relatively constant and oscillated around ca. 0.125 s^{-1} in the broad Co loading range. Only the catalyst with the lowest cobalt content displayed a significantly lower TOF. It was attributed to the decrease of the average cobalt particle size below the optimum of 20 nm. The decrease in size entailed the exponential growth of uncoordinated structures on the particle surface composed of strong hydrogen-binding sites, as the cobalt particles are composed of a face-centred cubic phase regardless of the size. The surface state of high-energy binding sites predominance leads to the poisoning of the cobalt surface with hydrogen under the ammonia synthesis reaction conditions. Hence, the activity is limited by blocking of the active sites for nitrogen adsorption, thus inhibiting the rate-determining step of the process.

Author Contributions: Conceptualization, W.P., M.Z. and W.R.-P.; methodology, W.P., M.Z. and W.R.-P.; investigation, W.P., A.F., A.A., D.M., P.D., M.Z., H.R., G.G. and W.R.-P.; writing—original draft preparation, W.P., M.Z.; writing—review and editing, W.P., M.Z. and W.R.-P.; visualisation, W.P.; supervision, W.P., M.Z. and W.R.-P. All authors have read and agreed to the published version of the manuscript.

Funding: This research received no external funding.

Data Availability Statement: All data is available within the paper.

Conflicts of Interest: The authors declare no conflict of interest.

References

- Smith, C.; Hill, A.K.; Torrente-Murciano, L. Current and future role of Haber–Bosch ammonia in a carbon-free energy landscape. *Energy Environ. Sci.* **2020**, *13*, 331–344. [\[CrossRef\]](#)
- Jennings, J.R. *Catalytic Ammonia Synthesis—Fundamentals and Practice*; Springer: New York, NY, USA, 2008.
- Liu, H. *Ammonia Synthesis Catalysts*; World Scientific: Singapore, 2013.
- Faria, J.A. Renaissance of ammonia synthesis for sustainable production of energy and fertilizers. *Curr. Opin. Green Sustain. Chem.* **2021**, *29*, 100466. [\[CrossRef\]](#)
- Nilsson, A.; Pettersson, L.G.M.; Hammer, B.; Bligaard, T.; Christensen, C.H.; Nørskov, J.K. The electronic structure effect in heterogeneous catalysis. *Catal. Lett.* **2005**, *100*, 111–114. [\[CrossRef\]](#)
- Hagen, S.; Barfod, R.; Fehrmann, R.; Jacobsen, C.J.H.H.; Teunissen, H.T.; Ståhl, K.; Chorkendorff, I. New efficient catalyst for ammonia synthesis: Barium-promoted cobalt on carbon. *Chem. Commun.* **2002**, *11*, 1206–1207. [\[CrossRef\]](#)
- Hagen, S.; Barfod, R.; Fehrmann, R.; Jacobsen, C.J.H.; Teunissen, H.T.; Chorkendorff, I. Ammonia synthesis with barium-promoted iron-cobalt alloys supported on carbon. *J. Catal.* **2003**, *214*, 327–335. [\[CrossRef\]](#)
- Raróg-Pilecka, W.; Miśkiewicz, E.; Kepiński, L.; Kaszkur, Z.; Kielar, K.; Kowalczyk, Z. Ammonia synthesis over barium-promoted cobalt catalysts supported on graphitised carbon. *J. Catal.* **2007**, *249*, 24–33. [\[CrossRef\]](#)
- Karolewska, M.; Truszkiewicz, E.; Wcisłowski, M.; Mierzwa, B.; Kepiński, L.; Raróg-Pilecka, W. Ammonia synthesis over a Ba and Ce-promoted carbon-supported cobalt catalyst. Effect of the cerium addition and preparation procedure. *J. Catal.* **2013**, *303*, 130–134. [\[CrossRef\]](#)
- Lin, B.; Qi, Y.; Wei, K.; Lin, J. Effect of pretreatment on ceria-supported cobalt catalyst for ammonia synthesis. *RSC Adv.* **2014**, *4*, 38093. [\[CrossRef\]](#)
- Lin, B.; Liu, Y.; Heng, L.; Ni, J.; Lin, J.; Jiang, L. Effect of ceria morphology on the catalytic activity of Co/CeO₂ catalyst for ammonia synthesis. *Catal. Commun.* **2017**, *101*, 15–19. [\[CrossRef\]](#)
- Lin, B.; Liu, Y.; Heng, L.; Ni, J.; Lin, J.; Jiang, L. Effect of barium and potassium promoter on Co/CeO₂ catalysts in ammonia synthesis. *J. Rare Earths* **2018**, *36*, 703–707. [\[CrossRef\]](#)
- Sato, K.; Miyahara, S.; Tsujimaru, K.; Wada, Y.; Toriyama, T.; Yamamoto, T.; Matsumura, S.; Inazu, K.; Mohri, H.; Iwasa, T.; et al. Barium Oxide Encapsulating Cobalt Nanoparticles Supported on Magnesium Oxide: Active Non-Noble Metal Catalysts for Ammonia Synthesis under Mild Reaction Conditions. *ACS Catal.* **2021**, *11*, 13050–13061. [\[CrossRef\]](#)
- Ronduda, H.; Zybert, M.; Patkowski, W.; Tarka, A.; Jodłowski, P.; Kepiński, L.; Sarnecki, A.; Moszyński, D.; Raróg-Pilecka, W. Tuning the catalytic performance of Co/Mg-La system for ammonia synthesis via the active phase precursor introduction method. *Appl. Catal. A Gen.* **2020**, *598*, 117553. [\[CrossRef\]](#)
- Ronduda, H.; Zybert, M.; Patkowski, W.; Tarka, A.; Ostrowski, A.; Raróg-Pilecka, W. Kinetic studies of ammonia synthesis over a barium-promoted cobalt catalyst supported on magnesium–lanthanum mixed oxide. *J. Taiwan Inst. Chem. Eng.* **2020**, *114*, 241–248. [\[CrossRef\]](#)
- Ronduda, H.; Zybert, M.; Patkowski, W.; Ostrowski, A.; Jodłowski, P.; Szymański, D.; Kepiński, L.; Raróg-Pilecka, W. Boosting the Catalytic Performance of Co/Mg/La Catalyst for Ammonia Synthesis by Selecting a Pre-Treatment Method. *Catalysts* **2021**, *11*, 941. [\[CrossRef\]](#)
- Ronduda, H.; Zybert, M.; Patkowski, W.; Ostrowski, A.; Jodłowski, P.; Szymański, D.; Kepiński, L.; Raróg-Pilecka, W. A high performance barium-promoted cobalt catalyst supported on magnesium–lanthanum mixed oxide for ammonia synthesis. *RSC Adv.* **2021**, *11*, 14218–14228. [\[CrossRef\]](#)
- Ronduda, H.; Zybert, M.; Patkowski, W.; Ostrowski, A.; Jodłowski, P.; Szymański, D.; Kepiński, L.; Raróg-Pilecka, W. Development of cobalt catalyst supported on MgO–Ln₂O₃ (Ln = La, Nd, Eu) mixed oxide systems for ammonia synthesis. *Int. J. Hydrog. Energy* **2022**, *47*, 6666–6678. [\[CrossRef\]](#)
- Inoue, Y.; Kitano, M.; Tokunari, M.; Taniguchi, T.; Ooya, K.; Abe, H.; Niwa, Y.; Sasase, M.; Hara, M.; Hosono, H. Direct Activation of Cobalt Catalyst by 12CaO₇Al₂O₃ Electride for Ammonia Synthesis. *ACS Catal.* **2019**, *9*, 1670–1679. [\[CrossRef\]](#)
- Gao, W.; Wang, P.; Guo, J.; Chang, F.; He, T.; Wang, Q.; Wu, G.; Chen, P. Barium Hydride-Mediated Nitrogen Transfer and Hydrogenation for Ammonia Synthesis: A Case Study of Cobalt. *ACS Catal.* **2017**, *7*, 3654–3661. [\[CrossRef\]](#)
- Raróg-Pilecka, W.; Karolewska, M.; Truszkiewicz, E.E.; Iwanek, E.; Mierzwa, B. Cobalt Catalyst Doped with Cerium and Barium Obtained by Co-Precipitation Method for Ammonia Synthesis Process. *Catal. Lett.* **2011**, *141*, 678–684. [\[CrossRef\]](#)

22. Tarka, A.; Patkowski, W.; Zybert, M.; Ronduda, H.; Wieciński, P.; Adamski, P.; Sarnecki, A.; Moszyński, D.; Raróg-Pilecka, W. Synergistic interaction of cerium and barium—new insight into the promotion effect in cobalt systems for ammonia synthesis. *Catalysts* **2020**, *10*, 658. [\[CrossRef\]](#)
23. Zybert, M.; Wyszynska, M.; Tarka, A.; Patkowski, W.; Ronduda, H.; Mierzwa, B.; Kepiński, L.; Sarnecki, A.; Moszyński, D.; Raróg-Pilecka, W. Surface enrichment phenomenon in the Ba-doped cobalt catalyst for ammonia synthesis. *Vacuum* **2019**, *168*, 108831. [\[CrossRef\]](#)
24. Patkowski, W.; Kowalik, P.; Antoniuk-Jurak, K.; Zybert, M.; Ronduda, H.; Mierzwa, B.; Próchniak, W.; Raróg-Pilecka, W. On the Effect of Flash Calcination Method on the Characteristics of Cobalt Catalysts for Ammonia Synthesis Process. *Eur. J. Inorg. Chem.* **2021**, *2021*, 1518–1529. [\[CrossRef\]](#)
25. Karolewska, M.; Truszkiewicz, E.; Mierzwa, B.; Kepiński, L.; Raróg-Pilecka, W. Ammonia synthesis over cobalt catalysts doped with cerium and barium. Effect of the ceria loading. *Appl. Catal. A Gen.* **2012**, *445–446*, 280–286. [\[CrossRef\]](#)
26. Zybert, M.; Tarka, A.; Mierzwa, B.; Kepiński, L.; Raróg-Pilecka, W. Promotion effect of lanthanum on the Co/La/Ba ammonia synthesis catalysts—The influence of lanthanum content. *Appl. Catal. A Gen.* **2016**, *515*, 16–24. [\[CrossRef\]](#)
27. Zybert, M.; Tarka, A.; Patkowski, W.; Ronduda, H.; Mierzwa, B.; Kepiński, L.; Raróg-Pilecka, W. Structure Sensitivity of Ammonia Synthesis on Cobalt: Effect of the Cobalt Particle Size on the Activity of Promoted Cobalt Catalysts Supported on Carbon. *Catalysts* **2022**, *12*, 1285. [\[CrossRef\]](#)
28. Ronduda, H.; Zybert, M.; Patkowski, W.; Sobczak, K.; Moszyński, D.; Albrecht, A.; Sarnecki, A.; Raróg-Pilecka, W. On the effect of metal loading on the performance of Co catalysts supported on mixed MgO–La₂O₃ oxides for ammonia synthesis. *RSC Adv.* **2022**, *12*, 33876–33888. [\[CrossRef\]](#)
29. Niwa, Y.; Aika, K. The Effect of Lanthanide Oxides as a Support for Ruthenium Catalysts in Ammonia Synthesis. *J. Catal.* **1996**, *162*, 138–142. [\[CrossRef\]](#)
30. Miyahara, S.I.; Sato, K.; Kawano, Y.; Imamura, K.; Ogura, Y.; Tsujimaru, K.; Nagaoka, K. Ammonia synthesis over lanthanoid oxide-supported ruthenium catalysts. *Catal. Today* **2020**, *376*, 2–5. [\[CrossRef\]](#)
31. Sato, K.; Imamura, K.; Kawano, Y.; Miyahara, S.; Yamamoto, T.; Matsumura, S.; Nagaoka, K. A low-crystalline ruthenium nano-layer supported on praseodymium oxide as an active catalyst for ammonia synthesis. *Chem. Sci.* **2017**, *8*, 674–679. [\[CrossRef\]](#)
32. Imamura, K.; Miyahara, S.I.; Kawano, Y.; Sato, K.; Nakasaka, Y.; Nagaoka, K. Kinetics of ammonia synthesis over Ru/Pr₂O₃. *J. Taiwan Inst. Chem. Eng.* **2019**, *105*, 50–56. [\[CrossRef\]](#)
33. Bernal, S.; Botana, F.J.; García, R.; Rodríguez-Izquierdo, J.M. Behaviour of rare earth sesquioxides exposed to atmospheric carbon dioxide and water. *React. Solids* **1987**, *4*, 23–40. [\[CrossRef\]](#)
34. Bernal, S.; Botana, F.J.; García, R.; Rodríguez-Izquierdo, J.M. Study of the interaction of two hexagonal neodymium oxides with atmospheric CO₂ and H₂O. *J. Mater. Sci.* **1988**, *23*, 1474–1480. [\[CrossRef\]](#)
35. Turcotte, R.P.; Sawyer, J.O.; Eyring, L. Rare earth dioxymonocarbonates and their decomposition. *Inorg. Chem.* **1969**, *8*, 238–246. [\[CrossRef\]](#)
36. Biesinger, M.C.; Payne, B.P.; Grosvenor, A.P.; Lau, L.W.M.; Gerson, A.R.; Smart, R.S.C. Resolving surface chemical states in XPS analysis of first row transition metals, oxides and hydroxides: Cr, Mn, Fe, Co and Ni. *Appl. Surf. Sci.* **2011**, *257*, 2717–2730. [\[CrossRef\]](#)
37. Garces, L.J.; Hincapie, B.; Zerger, R.; Suib, S.L. The Effect of Temperature and Support on the Reduction of Cobalt Oxide: An in Situ X-ray Diffraction Study. *J. Phys. Chem. C* **2015**, *119*, 5484–5490. [\[CrossRef\]](#)
38. Zybert, M.; Karasińska, M.; Truszkiewicz, E.; Mierzwa, B.; Raróg-Pilecka, W. Properties and activity of the cobalt catalysts for NH₃ synthesis obtained by co-precipitation—the effect of lanthanum addition. *Pol. J. Chem. Technol.* **2015**, *17*, 138–143. [\[CrossRef\]](#)
39. Ciufu, R.A.; Han, S.; Floto, M.E.; Eichler, J.E.; Henkelman, G.; Mullins, C.B. Hydrogen desorption from the surface and subsurface of cobalt. *Phys. Chem. Chem. Phys.* **2020**, *22*, 15281–15287. [\[CrossRef\]](#)
40. Huesges, Z.; Christmann, K. Interaction of Hydrogen with a Cobalt(0001) Surface. *Z. Für Phys. Chem.* **2013**, *227*, 881–899. [\[CrossRef\]](#)
41. Kitakami, O.; Sato, H.; Shimada, Y.; Sato, F.; Tanaka, M. Size effect on the crystal phase of cobalt fine particles. *Phys. Rev. B* **1997**, *56*, 13849–13854. [\[CrossRef\]](#)
42. Liu, J.X.; Li, W.X. Theoretical study of crystal phase effect in heterogeneous catalysis. *Wiley Interdiscip. Rev. Comput. Mol. Sci.* **2016**, *6*, 571–583. [\[CrossRef\]](#)
43. Freels, M.; Liaw, P.K.; Jiang, L.; Klarstrom, D.L. Advanced Structural Materials: Properties, Design Optimization, and Applications. In *Advanced Structural Materials: Properties, Design Optimization, and Applications*; Soboyejo, W.O., Srivatsan, T.S., Eds.; CRC Press: Boca Raton, FL, USA, 2007; pp. 187–224.
44. Weststrate, C.J.; Mahmoodinia, M.; Farstad, M.H.; Svenum, I.-H.; Strømsheim, M.D.; Niemantsverdriet, J.W.; Venvik, H.J. Interaction of hydrogen with flat (0001) and corrugated (11–20) and (10–12) cobalt surfaces: Insights from experiment and theory. *Catal. Today* **2020**, *342*, 124–130. [\[CrossRef\]](#)
45. Weststrate, C.J.; Garcia Rodriguez, D.; Sharma, D.; Niemantsverdriet, J.W. Structure-dependent adsorption and desorption of hydrogen on FCC and HCP cobalt surfaces. *J. Catal.* **2022**, *405*, 303–312. [\[CrossRef\]](#)
46. Fernández, C.; Bion, N.; Gaigneaux, E.M.; Duprez, D.; Ruiz, P. Kinetics of hydrogen adsorption and mobility on Ru nanoparticles supported on alumina: Effects on the catalytic mechanism of ammonia synthesis. *J. Catal.* **2016**, *344*, 16–28. [\[CrossRef\]](#)
47. Kojima, R.; Aika, K. Cobalt molybdenum bimetallic nitride catalysts for ammonia synthesis. *Appl. Catal. A Gen.* **2001**, *218*, 121–128. [\[CrossRef\]](#)

48. Rosowski, F.; Hornung, A.; Hinrichsen, O.; Herein, D.; Muhler, M.; Ertl, G. Ruthenium catalysts for ammonia synthesis at high pressures: Preparation, characterization, and power-law kinetics. *Appl. Catal. A Gen.* **1997**, *151*, 443–460. [[CrossRef](#)]
49. Rivera Rocabado, D.S.; Aizawa, M.; Noguchi, T.G.; Yamauchi, M.; Ishimoto, T. Uncovering the Mechanism of the Hydrogen Poisoning on Ru Nanoparticles via Density Functional Theory Calculations. *Catalysts* **2022**, *12*, 331. [[CrossRef](#)]
50. Boudart, M. Kinetics and mechanism of ammonia synthesis. *Catal. Rev. Eng.* **1981**, *23*, 1–15. [[CrossRef](#)]
51. Ertl, G.; Lee, S.B.; Weiss, M. Adsorption of nitrogen on potassium promoted Fe(111) and (100) surfaces. *Surf. Sci.* **1982**, *114*, 527–545. [[CrossRef](#)]
52. Bozso, F.; Ertl, G.; Grunze, M.; Weiss, M. Chemisorption of hydrogen on iron surfaces. *Appl. Surf. Sci.* **1977**, *1*, 103–119. [[CrossRef](#)]
53. Ertl, G. Surface Science and Catalysis—Studies on the Mechanism of Ammonia Synthesis: The P. H. Emmett Award Address. *Catal. Rev.* **1980**, *21*, 201–223. [[CrossRef](#)]
54. Rosynek, M.P. Catalytic Properties of Rare Earth Oxides. *Catal. Rev.—Sci. Eng.* **1977**, *16*, 111–154. [[CrossRef](#)]
55. Alvero, R.; Odriozola, J.A.; Trillo, J.M.; Bernal, S. Lanthanide oxides: Preparation and ageing. *J. Chem. Soc. Dalt. Trans.* **1984**, *2*, 87. [[CrossRef](#)]
56. Bernal, S.; Blanco, G.; Calvino, J.J.; Omil, J.A.P.; Pintado, J.M. Some major aspects of the chemical behavior of rare earth oxides: An overview. *J. Alloy. Compd.* **2006**, *408–412*, 496–502. [[CrossRef](#)]
57. Reuel, R.C.; Bartholomew, C.H. The stoichiometries of H₂ and CO adsorptions on cobalt: Effects of support and preparation. *J. Catal.* **1984**, *85*, 63–77. [[CrossRef](#)]
58. Borodziński, A.; Bonarowska, M. Relation between Crystallite Size and Dispersion on Supported Metal Catalysts. *Langmuir* **1997**, *13*, 5613–5620. [[CrossRef](#)]
59. Kowalczyk, Z. Effect of potassium on the high pressure kinetics of ammonia synthesis over fused iron catalyst. *Catal. Lett.* **1996**, *37*, 173–179. [[CrossRef](#)]

Disclaimer/Publisher’s Note: The statements, opinions and data contained in all publications are solely those of the individual author(s) and contributor(s) and not of MDPI and/or the editor(s). MDPI and/or the editor(s) disclaim responsibility for any injury to people or property resulting from any ideas, methods, instructions or products referred to in the content.